Landsat-4 and Landsat-5 Thematic Mapper Data Quality Analysis

Erick Malaret, Luis A. Bartolucci, D. Fabian Lozano, Paul E. Anuta, and *Clare D. McGillem*
Laboratory for Applications of Remote Sensing, School of Electrical Engineering, Purdue University, West Lafayette, IN 47906

ABSTRACT: A Landsat Thematic Mapper quality evaluation study was conducted to determine the existence of geometric and radiometric sensor errors in data in the postlaunch environment. The study began with the launch of Landsat-4; several error conditions were found, including band-to-band geometric misregistration and detector-to-detector radiometric calibration errors. These results were reported and used by NASA to update the system.

This paper describes similar analysis for the Landsat-5 Thematic Mapper, and comparisons are made with results for Landsat-4. Remaining band-to-band misregistration was found to be within tolerances and detector-to-detector calibration errors were not severe but still existent. More coherent noise signals were observed in TM-5 than in TM-4, although the amplitude was generally less. The scan-direction differences observed in TM-4 were still evident in TM-5, the largest effect being in band 4 where nearly a one digital count difference was observed. Resolution estimation was carried out using roads in TM-5 for the primary focal plane bands rather than field edges as in TM-4. Thermal IR band calibration studies were conducted and new nonlinear calibration procedures were defined for TM-5. The overall conclusion is that there are no first-order errors in TM-5 and any remaining problems are second or third order.

INTRODUCTION

THIS PAPER DESCRIBES ANALYSES of Landsat-5 Thematic Mapper (TM-5) data to evaluate geometric and radiometric quality. In a previous paper (Anuta *et al.*, 1984), Landsat-4 Thematic Mapper (TM-4) and Multispectral Scanner (MSS) data were analyzed for the geometric and radiometric quality and information content. The results of the Landsat-5 work are compared to that for the Landsat-4. Not all the topics studied in the Landsat-4 study were repeated, therefore only a subset of the results are comparable. As a guide to the results in the two papers, the subjects are listed below with those reported in this paper indicated in the second column.

The results of the Landsat-4 study revealed several geometric and radiometric errors which, when reported to the National Aeronautics and Space Administration (NASA) by the authors and also by several other investigators, resulted in corrections and modifications that were incorporated in Landsat-4 ground processing and the Landsat-5 sensors. This study is a final evaluation of the success of these changes, and the results indicate no significant problems with the TM system. Some second-order problems with noise and calibration exist, and these are discussed.

DATA SETS

Landsat data from two sites were used in this study, one in northern Iowa and the other covering

	IEEE GRS* May 84	ASPRS Sept. 85
1. Effects of resampling (comparison of A & P tapes)	X	
2. Band-to-band registration	X	X
3. Detector-to-detector calibration	X	X
4. Coherent-noise analysis	X	X
5. Spatial resolution estimation	X	X
6. Scan-angle effects	X	
7. Scan-direction effects	X	X
8. Spectral dimensionality	X	
9. Spectral separability	X	
10. Thermal calibration	X	X

* Anuta *et al.*, 1984.

PHOTOGRAMMETRIC ENGINEERING AND REMOTE SENSING, Vol. 51, No. 9, September 1985, pp. 1407-1416.

0099-1112/85/5109-1407$02.25/0

the Chicago, IL area. The Landsat-4 data are frames 40049-16264 on 3 September 1982 for Iowa and 40101-16025 on 25 October 1982 for Illinois. The Landsat-5 data are frames 50151-16290 on 30 July 1984 for Iowa and 50139-16035 on 18 July 1984 for Illinois.

BAND-TO-BAND MISREGISTRATION

The importance of band-to-band registration is that it specifies the spatial alignment of all spectral bands in the system. Exact requirements for band-to-band misregistration were as follows (Landsat-D Application Notice, 1981).

> A point imaged in any of the first four spectral bands shall be registered to the same point in any of the other first four spectral bands within .2 IFOV along-track and across-track. This registration error includes the effects of all synchronizing and correcting signals developed by the instrument that are required to process the data into an image. Similarly Bands 5 and 7 shall be registered within .2 pixel and shall be registered to Band 6 within .2 of a Band 6 IFOV, and Band 5 shall be registered to the first four bands within .3 IFOV. These requirements shall be satisfied at least 90% of the time and apply to all points along a scan line.

Visual blink comparison of the different bands in both TM-4 and TM-5 showed registration accuracy was extremely good; detailed analysis was required to find subtle errors.

Band-to-band misregistration was assessed using a correlation algorithm capable of estimating shifts to subpixel accuracy and which could be applied row-wise or column-wise. The algorithm found the lag at which the correlation coefficient between any two bands was maximum by using cubic spline interpolation. It was found that better results were obtained if the registration algorithm was applied to images in which discontinuities were enhanced by some kind of gradient operation technique. The gradient operation used was implemented as follows: if g_i corresponded to the image plane of band i, then for across-track measurements of misregistration, every row in g_i was convolved with

$$[-1 \; 1 \; 0]$$

and the magnitude of the resulting image was taken. This is equivalent to computing the magnitude of the gradient along the rows of g_i. The advantage of this is that it enhances all the boundaries and sharp discontinuities in the image, which is exactly the kind of scene features an observer uses when evaluating misregistration by visual inspection. The gradient operator was applied row-wise for estimating the registration in the across-track direction or column-wise for the along-track direction.

The means and standard deviations of the shifts for blocks of 64 × 256 pixels were computed using P-tape data from Illinois for both TM-4 and TM-5. Misregistration for the TM-4 had been previously assessed (Anuta *et al.*, 1984), and the possible existence of misregistration problems between the primary focal plane bands (bands 1 through 4) and bands 5 and 7 was reported. More recent results obtained for TM-4 by preprocessing the data with a gradient operator indicate that bands 1 through 4 are registered within the tolerance limits with bands 5 and 7. Band pairs 4-1 and 4-3 gave misregistration of at most 0.38 pixel, which is above the tolerance limit of 0.2 IFOV. This misregistration could result from the observed poor correlation between bands 1-3 with band 4 and therefore is not necessarily conclusive.

For TM-5 we found that the first four bands, which lie in the primary focal plane, have a mean misregistration of, at most, 0.07 pixel, which is well within the 0.2 pixel specification. Results for the estimated across- and along-track registration for TM-5 are presented in Table 1 and Table 2, where X_{ij} is the mean misregistration between bands i and

TABLE 1. TM-5 MISREGISTRATION IN THE ACROSS-TRACK DIRECTION OVER A 25 × 64 PIXEL BLOCK IN ILLINOIS P-DATA. UNITS ARE TM REFLECTIVE BAND PIXELS

Band		1	2	3	4	5	7	6
1		0.00	0.00	0.00	0.06	0.04	0.02	0.32
2			0.00	0.00	0.07	0.02	0.01	0.45
3				0.00	0.06	0.02	0.01	0.49
4	$[X_{ij}]$ =				0.00	−0.02	−0.02	−0.30
5						0.00	−0.01	0.04
7							0.00	−0.32
6								0.00
1		0.00	0.06	0.07	0.21	0.16	0.14	2.76
2			0.00	0.02	0.19	0.11	0.12	2.71
3				0.00	0.12	0.08	0.10	2.68
4	$[\sigma_{X_{ij}}]$ =				0.00	0.12	0.08	1.70
5						0.00	0.07	1.85
7							0.00	1.62
6								0.00

TABLE 2. TM-5 MISREGISTRATION IN THE ALONG-TRACK DIRECTION OVER A 64 × 256 PIXEL BLOCK IN ILLINOIS P-DATA

Band		1	2	3	4	5	7	6
1		0.00	0.01	0.01	−0.06	0.07	0.06	0.36
2			0.00	0.01	0.00	0.05	0.04	0.67
3				0.00	−0.01	0.02	0.01	0.40
4	$[X_{ij}]$ =				0.00	0.05	0.06	0.14
5						0.00	−0.01	0.00
7							0.00	−0.25
6								0.00
1		0.00	0.03	0.02	0.53	0.17	0.15	1.85
2			0.00	0.02	0.23	0.12	0.11	1.82
3				0.00	0.07	0.10	0.09	2.01
4	$[\sigma_{X_{ij}}]$ =				0.00	0.19	0.12	1.89
5						0.00	0.03	1.79
7							0.00	1.31
6								0.00

j, and $\sigma_{X_{ij}}$ is the corresponding standard deviation. Overall, the TM-5 complies very well with all the registration requirements for both along- and across-track directions.

STRIPING EFFECTS

There are two basic types of striping effects that have been observed on TM-4 and TM-5 imagery. These are detector-to-detector striping and scan-to-scan striping (also called banding). The first is due to gain differences between the detectors in any given band, and the second to alternating levels of brightness related to the forward and reverse scanning operations.

TM-5 detector-to-detector striping and banding was assessed by computing the mean values for 256 consecutive scanlines of P-tape data* over a Lake Michigan scene (18 July 1984). Means for 16 groups of lines taken at intervals of 16 lines were computed to obtain detector-related means. Since A-tape data were not available, we assumed that no line insertions occurred in the 256-line interval. The validity of this could not be evaluated. This area was selected because of the low intensity level and small variation present in the signal, facilitating the study of banding and striping phenomena. Figures 1 and 2 show results obtained for TM-5 bands 4 and 7. In bands 4 and 7, the banding phenomenon was clearly seen, with an average difference between scans of approximately 0.9 and 0.51 binary number, respectively. In band 4 the difference was almost one binary number, which made it easily noticeable by visual inspection. Striping was also noticeable in these two bands. Band 5 showed striping formed mainly by a single detector, with a standard deviation of approximately 0.8 binary number. Also bands 6 and 7 showed evidence of striping. In band 2 an oscillation with a period of approximately 256 scan lines was observed. The differences in binary number observed in the TM-5 due to banding and striping were all less than 1, indicating that relative calibration was very good.

For TM-4, banding and striping effects were also studied over the same area of Lake Michigan. In TM-4 banding was observed only on band 4, while striping was present in all other bands. The striping observed in bands 7, 5, 3, and 1 was due mainly to a single detector. With the exception of band 7, the banding and striping deviation was below the one binary number range. For band 7 striping due to a single detector was in some cases as big as 1.1 binary number.

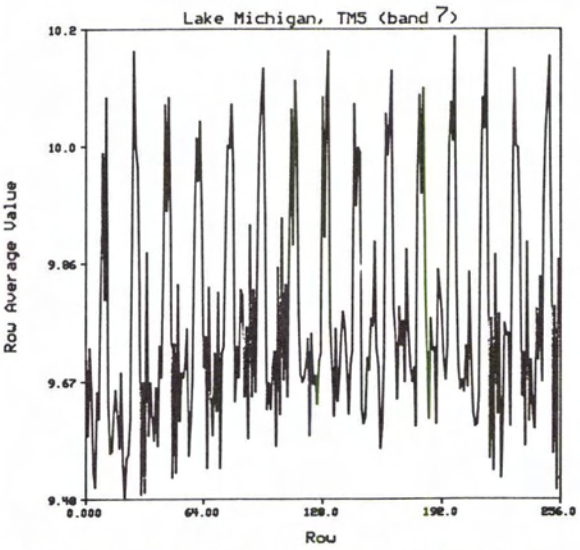

FIG. 1. Scanline averaging for low-level TM-5 band 4 data over a 256 × 256 block showing scan-to-scan striping.

* A-tape data were not available for the study.

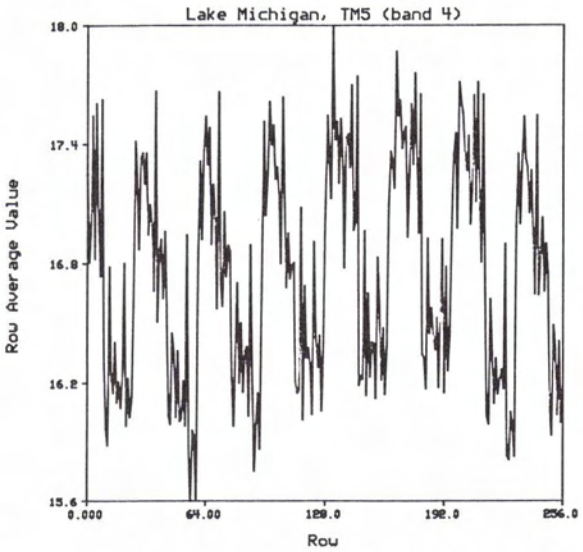

FIG. 2. Scanline averaging for low-level TM-5 band 7 data over a 256 × 256 block showing detector-to-detector striping.

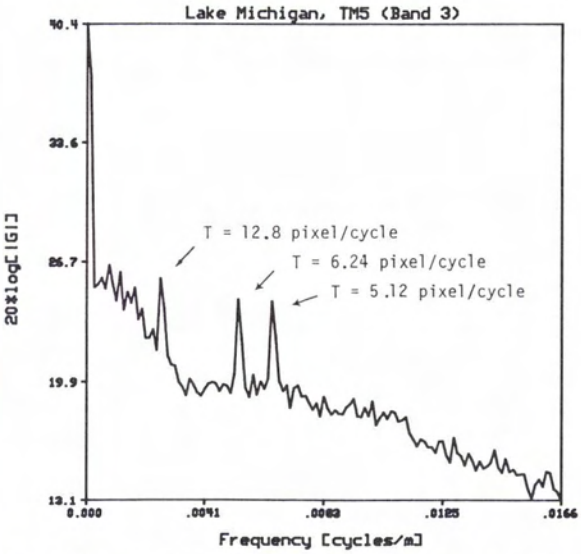

FIG. 3. Power spectrum of low-level TM-5 data showing noise peaks at 5.12, 6.24, 12.8 pixel/cycle. Frequency axis is in cycles per meter for P-tape pixel spacing (28.5 μm).

COHERENT NOISE ANALYSIS

Presence of coherent noise in the TM-4 has been reported previously (Anuta *et al.*, 1984; Bernstein *et al.*, 1984). The source of this noise is believed to be related to specific electronic or mechanical oscillations in the system. TM-5 P-data were searched for the presence of coherent noise sources. An average power spectrum was estimated over a block of 256 × 256 pixels in Lake Michigan. The power spectrum measurement used is given by

$$20 \log_{10} \left[\frac{1}{N} \sum_{i=1}^{256} DFT(w_{ij} g_{ij}) \right] \quad 1 \leq j \leq 256 \qquad (1)$$

where g_{ij} is the image with corresponding row and column index i, j and w_{ij} is a Hamming window function, and *DFT* signifies the discrete Fourier transform. The Hamming function is described in McGillem *et al.* (1974), p. 162. Figure 3 shows the estimated power spectrum for TM band 3, where the presence of three noise frequencies can be easily seen with corresponding periods of 12.8, 6.24, and 5.12 pixels. The power in the TM-5 noise frequencies is nominally 5 to 7 db above the background noise level in bands 2, 3, 4, 5, and 7.

Table 3 compiles the different noise periods measured for data acquired over Lake Michigan in both the TM-5 and TM-4. The measured noise periods in the TM-4 and TM-5 are not the same. The observed periods were too low to be attributed to jitter. No in-depth attempt was made here to find the source of this noise. Results are presented as evidence to aid researchers and data processing agencies in correcting for these anomalies.

RESOLUTION ESTIMATION IN TM DATA

One geometric parameter of particular interest is the actual in-flight resolution of the sensor system which includes all environmental and data processing factors. The resolution is determined by the point-spread function (PSF) of the system. This can be estimated in image data by observing the measured response to scene elements of known shape.

For a space-invariant PSF, the measured image in the spatial domain can be expressed as a convolution of the scene with the PSF, i.e.,

$$g(x,y) = h(x,y) * f(x,y) \qquad (2)$$

where $f(x,y)$ is the Earth scene, $h(x,y)$ is the overall PSF of the sensor system, and $g(x,y)$ is the resulting image.

TABLE 3. COHERENT NOISE PERIODS (IN PIXEL CYCLE) USING LAKE MICHIGAN DATA

Band	TM-4	TM-5
1	17, 3.12	none
2	17, 3.12	6.24
3	17, 3.12	12.8, 6.24, 5.12
4	17, 3.12	5.12
5	3.12 hardly noticeable	5.12
7	3.12 hardly noticeable	12.19, 5.12
6	none	none

Three scene elements that are useful for this type of analysis are:

1. An impulse represented by a narrow-width discontinuity along a row or column of the data, e.g., narrow roads.
2. A step function represented by an abrupt change in gray level along a row or column of the data.
3. A rectangular pulse represented by a sequence of two steps in opposite directions along a row or column of the data.

For our purposes, we estimated the line-spread function (LSF) in the direction normal to the discontinuity generated by any of the three suggested scene elements. If the LSF is known for many different orientation angles (Rosenfeld, 1982), then the two-dimensional PSF can be reconstructed.

It was observed by experimentation with the three types of scene elements that the step edge was the most desirable to use in bands 5 and 7. In particular, agricultural field edges with high contrast fields of uniform texture were used. For bands 1 through 4 the first type of scene element was used. To determine the LSF, subpixel sampling is required since the sample rate of the TM is nominally the width of the predicted LSF. A procedure was defined to allow subpixel sampling of edges or roads which is described in detail in Anuta *et al.* (1984). One critical aspect of the data extraction procedure is the accurate estimation of the scene element orientation, since any error here will propagate to the LSF estimate. Performance curves which relate the variance of the scene element orientation to the signal-to-noise ratio were obtained, and a discriminant function for scene element selection was developed (Malaret, 1984). The subpixel scheme was applied to scene elements in the Iowa and Illinois data sets. A set of response values at a large number of intersample locations was obtained for several scene elements in all bands, except band 6. For the case of field edges, the LSF was estimated in earlier work (McGillem *et al.*, 1983, 1984) using a finite sum of basis functions or by relating the derivative of the system response to the LSF.

When a narrow road is used for estimating the LSF, it can be modeled as a narrow-width discontinuity superimposed on a constant background, i.e.,

$$f(x) = A\,\mathrm{rect}\left(\frac{x}{\tau}\right) + B \tag{3}$$

where:

$\mathrm{rect}\,(x/\tau) = 1$ for $-1/2 \leq x/\tau \leq -1/2$, zero elsewhere

τ is the width of the road in pixels

A is the amplitude of the discontinuity

B is the constant background

The resolution of the TM is approximately 30 m; therefore, if rural area roads with a width of approximately 6 to 7 m are used, the system response can be used to establish upper bounds in the system resolution. The equivalent width of the LSF has been previously used to characterize the resolution of the TM. It is interesting to see how the equivalent width of the TM to a narrow road can be related to the equivalent width of the actual LSF. It can be shown (Malaret, 1984) that the exact relation is

$$W_{eq}(h) = \alpha W_{eq}(g) = \frac{1}{\tau}\int_{-\frac{\tau}{2}}^{\frac{\tau}{2}} \frac{h(\lambda)}{h(0)}\, d\lambda W_{eq}(g) \tag{4}$$

where α is less than or equal to 1 due to the monotonically decreasing behavior of the *LSF* away from the origin. Since we do not know h offhand, α is not known exactly. However, for the case of $\tau = 6$ m and h given by a Gaussian function with half amplitude width of 1, we obtain $\alpha = .995$. This convinced us that narrow roads can be used for estimating the system resolution capabilities as long as the half-amplitude width of h is approximately equal to or greater than 1. The estimated LSF is given by a smoothed representation of the system response to the road.

Scene elements for the two cases considered were extracted from the Iowa and Illinois scenes. Figures 4 and 5 show the raw data for bands 3 and 7. The resulting LSF, when cubic splines are used for smoothing, are shown in Figures 6 and 7. Table 4 is a compilation of the LSF half-amplitude widths estimates, using two types of smoothing algorithm, in the TM-5. The units used in this table are sam-

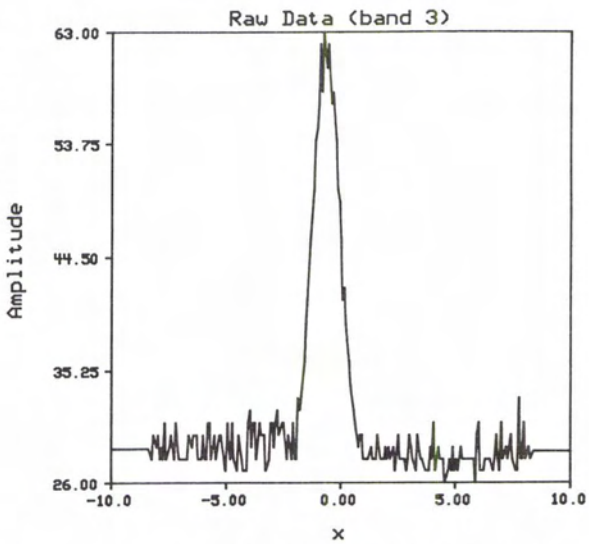

FIG. 4. Extracted road raw data from rural area in Illinois.

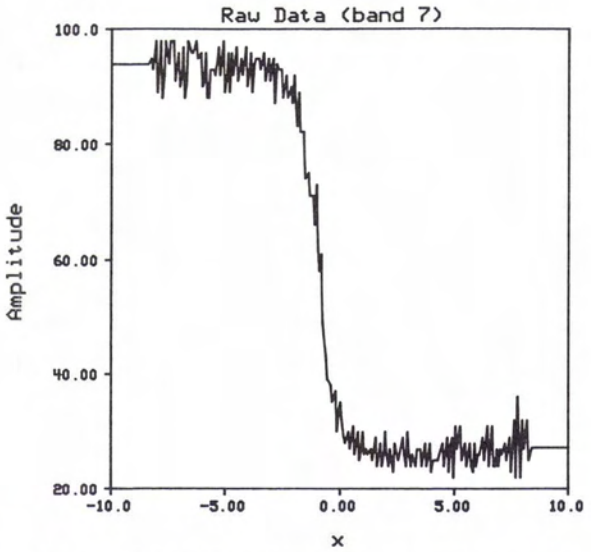

FIG. 5. Extracted step edge raw data from Illinois scene.

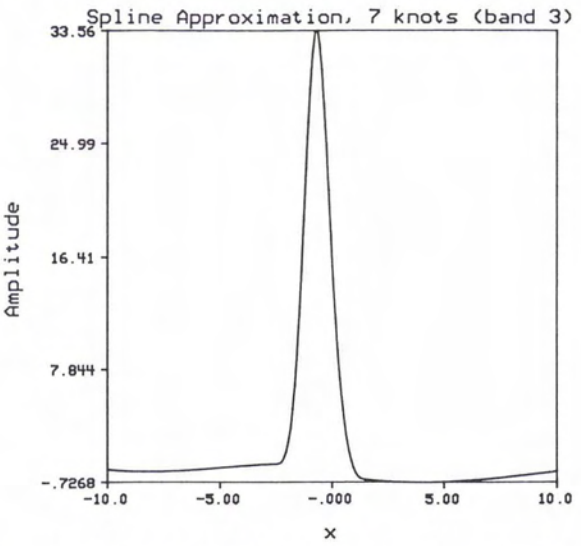

FIG. 7. Estimated LSF from the system response to a road for TM-5 band 3.

pling intervals (*si*), where one *si* = 28.5 m. As we concluded in earlier work for the TM-4, TM-5 resolution estimates also indicate that the actual overall resolution is slightly less than the joint electronic and optical system resolution of 1 IFOV. This may be due to atmospheric and data processing effects or to the characteristics of the scene elements used.

CALIBRATION OF LANDSAT-5 TM THERMAL IR DATA

The procedures for calibration of the Landsat-4 TM thermal IR data and the resulting water temperature maps have been reported in a previous paper (Anuta *et al.*, 1984). This paper deals with the calibration of the thermal IR data collected by the Thematic Mapper sensor on board Landsat-5, and it includes a description of the procedures developed for calibration, the results of calibrated thermal IR data, and a comparison of these procedures and results with those obtained from the Landsat TM-4 data.

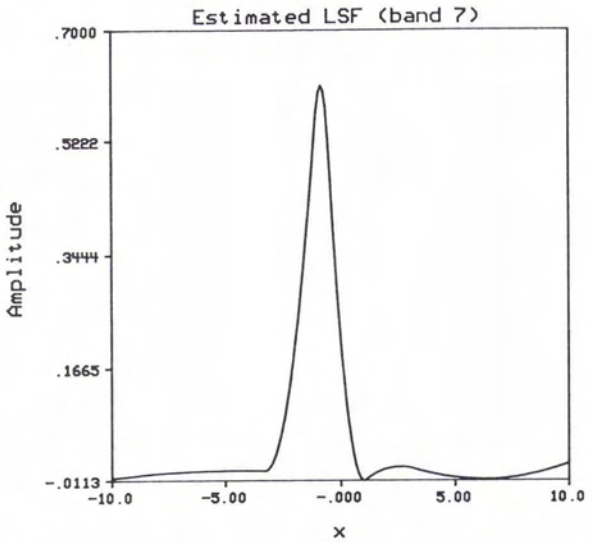

FIG. 6. Estimated LSF from step edge for TM-5 band 7.

CALIBRATION PROCEDURE

The calibration of the TM-4 thermal IR data was straightforward because the temperatures of the internal calibration sources (blackbodies) were known with good reliability, i.e., 260°K and 320°K, which corresponded to the 0 and 255 digital count levels, respectively. On the other hand, the temperatures of the reference blackbodies for the TM-5 sensor were not known with a high degree of accuracy (Hughes Aircraft Co., 1985). Therefore, the first step in the calibration procedure involved the determination of these two reference temperatures for the TM-5 sensor.

TABLE 4. RESULTS OF TM-5 RESOLUTION ESTIMATION IN TERMS OF HALF-AMPLITUDE WIDTH

Band	Trig. Smoothing, $W_{\frac{1}{2}}(si)$	Spline Smoothing, $W_{\frac{1}{2}}(si)$
1	1.42 *si*	1.25 *si*
2	1.20 *si*	1.16 *si*
3	1.42 *si*	1.31 *si*
4	1.50 *si*	1.06 *si*
5	1.33 *si*	1.34 *si*
7	1.37 *si*	1.49 *si*

si = sampling interval

To determine these temperatures, the minimum (R_{min}) and maximum (R_{max}) spectral radiances stored as radiometric calibration ancillary records on the P-tape CCTs (NASA: 1093, 1983) were used in conjunction with the results of the integration of Planck's equation for a bandwidth defined by the mean system response function of all four band-6 detectors. Table 5 shows the values (in mW/(cm^2 sr μm)) of the minimum and maximum spectral radiances corresponding to the 0 and 255 digital count levels for the thermal IR band data of the TM-5 scene no. 50139-16035.

These spectral radiances were then converted to in-band radiances for a band defined by the mean system response function of all four detectors. The system response curves for the four detectors of both the Landsat-4 (protoflight) and Landsat-5 (flight) sensors are illustrated in Figure 8, and the in-band R_{min} and R_{max} radiances are given in Table 6.

These R_{min} (in-band) and R_{max} (in-band) radiances correspond to the amount of energy emitted by a blackbody radiating at 203.2°K and 341.2°K, respectively, which should be the temperatures of the two internal calibration sources for the thermal IR band of the Landsat-5 Thematic Mapper sensor system, and they should correspond to the 0 and 255 digital count levels of the data.

Since the Thematic Mapper product (P-tape) data have been radiometrically corrected so that there is a linear relationship between radiance and the corresponding digital counts (DC), the following linear transformation was derived for the conversion of digital counts into in-band radiances and vice versa:

$$R(\text{In-Band}) = (DC + 21.977)/90.127 \qquad (5)$$

where:

R = In-band radiance in mW/cm^2 sr
DC = Digital counts between 0 and 255

Planck's equation was integrated between 10.00 μm and 13.00 μm at spectral intervals of 0.01 μm and for a range of temperatures between 203.2°K and 341.2°K. The resulting in-band radiances were then multiplied by the normalized relative (RSR) system response values (the mean for all four TM-5 detectors) given by Markham and Barker (1985), and then summed over the entire 10.00 μm and 13.00 μm temperature range, as illustrated by Equation (6).

$$W_{\overline{SR}} = \Sigma_i \left[\left(\int_{\lambda_L + i\Delta\lambda}^{\lambda_L + (i+1)\Delta\lambda} 2hc^2\lambda^{-5} \left(e^{hc/\lambda kT} - 1\right) d\lambda \right) \frac{-1}{SR_i} \right] \qquad (6)$$

TABLE 5. SPECTRAL R_{MIN} AND R_{MAX} FOR THE TM-5 THERMAL IR BAND

R_{min} (Spectral)	= 0.1237800 mW/(cm^2 sr μm)
R_{max} (Spectral)	= 1.5599560 mW/(cm^2 sr μm)

where:

W = In-band radiance in mW/cm^2 sr.
c = Speed of light
h = Planck's constant
λ = Wavelength
k = Boltzmann's constant
T = Temperature in degrees Kelvin
SR = System normalized relative response (Markham and Barker, 1985)
λ_L = 10 μm
$\Delta\lambda$ = .01 μm
i = 0–300

The in-band radiances derived from Equation (6) can be closely approximated by in-band radiances produced by a square band with lower and upper limits located at the 50 percent cutoff of the system response curve, i.e., 10.42 μm and 12.45 μm, respectively.

As reported by Bartolucci *et al.* (1973), the relationship between radiance (or digital counts) and temperature, for ranges of temperatures greater than 10°K is not linear; therefore a quadratic and a cubic fit were derived to convert the TM-5 thermal IR band digital counts into radiant temperatures. Figure 9 shows both the quadratic and cubic regression curves, and for illustration purposes only, the linear regression curve also is included in the figure. The linear, quadratic, and cubic regression models are given by the following expressions (Equations 7, 8, and 9):

Linear Model.

$$T(K) = 219.972 + 0.526\,DC \qquad (7)$$

Quadratic Model.

$$T(K) = 209.831 + 0.834\,DC - 0.00133\,DC^2 \qquad (8)$$

Cubic Model.

$$T(K) = 206.127 + 1.0545\,DC^2 - 0.00371\,DC + (6.606 \times 10^{-6})\,DC^3 \qquad (9)$$

Both quadratic (Equation 8) and cubic (Equation 9) models may be used to convert the TM-5 thermal IR band digital counts into radiant temperatures. However, depending upon the range of temperatures in question, one or the other model (either the quadratic or the cubic model) will better fit the actual data, as reported by Bartolucci *et al.* (1985).

Temperature Mapping of Water Bodies

To test the TM-5 thermal IR data calibration procedure, a Landsat-5 TM scene (ID: 50139-16035) collected on 18 July 1984 over the Chicago, IL region was utilized. First, a hierarchical classification was performed using data from the 1.55 μm to 1.75 μm middle IR band to separate the water pixels from all other ground cover types. Then, the relative thermal IR spectral response (digital counts) corresponding to water pixels was calibrated using Equations (7), (8), and (9). The resulting radiant

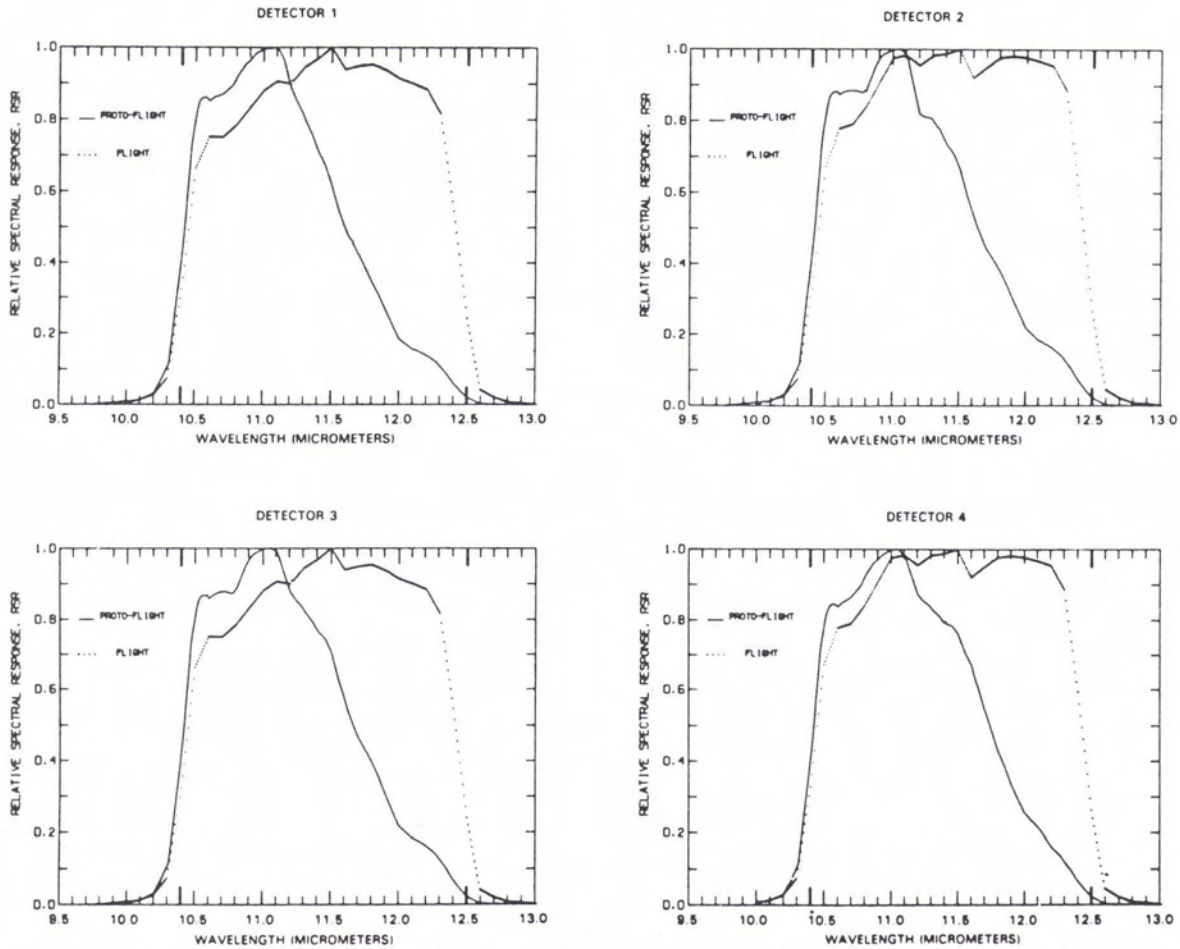

FIG. 8. System response curves for the landsat-4 (protoflight) and Landsat-5 (flight) thermal IR band detectors (after Markham and Barker, 1985).

temperatures of water were compared with reference temperatures measured at seven different locations (five in Lake Michigan and two in the Dresden nuclear power plant cooling lake). The Lake Michigan temperatures were measured by Chicago Park District personnel, and the reference temperatures for the Dresden cooling lake were optimized from records available at the Dresden power plant management office. Table 7 shows the radiant temperatures computed using the linear, quadratic, and cubic models, the original digital counts, the reference temperatures, and the radiant temperatures obtained from the integration of Planck's equation without using regression fits.

In Table 7 notice that the cubic model results show a better fit for the actual data or no-model temperatures, for a temperature range between 16.4°C and 30.2°C. Also the radiant temperatures (no-model temperature column) and the reference temperatures (ground temperature column) show a discrepancy in absolute values from a minimum of 0.3°C in Lake Michigan up to 2.4°C in the Dresden cooling lake. These discrepancies are to be expected because in this thermal IR data calibration procedure the atmospheric effects have not been taken into consideration.

Furthermore, the reference temperatures were obtained a few hours before and after the Landsat-5 TM sensor collected the thermal IR data. Nevertheless, these preliminary results indicate that

TABLE 6. IN-BAND R_{MIN} AND R_{MAX} FOR THE TM-5 THERMAL IR BAND

R_{min} (In-Band)	= 0.2438466 (mW/cm^2 sr)
R_{max} (In-Band)	= 3.0731133 (mW/cm^2 sr)

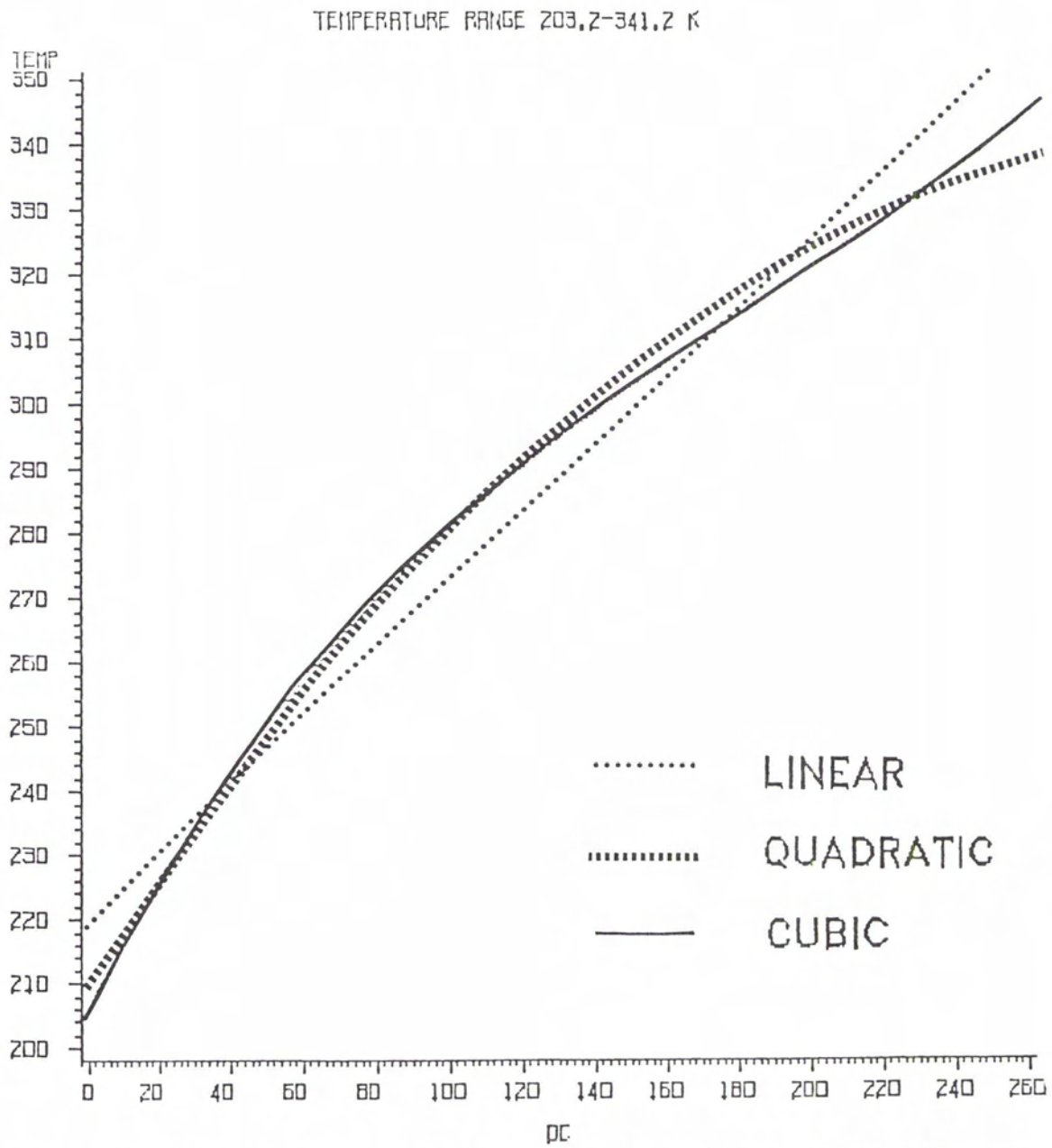

FIG. 9. Linear, quadratic, and cubic regression models for the relationship between digital counts and temperature for the Landsat-5 thermal IR band.

there is great potential for utilizing the relatively high spatial resolution thermal IR data from the Thematic Mapper sensors for measuring and mapping Earth surface temperatures with a high degree of accuracy and reliability.

Additional analyses of TM-5 thermal IR data in conjunction with more reliable measurements of reference temperatures and use of atmospheric effects correction models should be conducted before a final verdict is given for the Landsat TM thermal IR data collection capabilities.

SUMMARY AND CONCLUSIONS

This paper describes results of Landsat-4 and Landsat-5 sensor data quality analysis activities

which were carried out over a three-year period covering the Landsat-4 and Landsat-5 launches and deployment. The geometric and radiometric errors found in the TM-5 data were not large, and their effect on utilization of the data is considered to be small. The performance must be considered in terms of original specifications. For geometry, two parameters are most significant: band-to-band registration and large area geometric fidelity. Band-to-band registration tests indicate that all bands are within or near specification. Large area geometric accuracy evaluation is not reported in this paper.

Radiometric analysis indicates that some striping and scan-direction dependent banding still exists but with small amplitude. Banding is most severe in band 4 with nominally a one-count difference between east and west scans. Several coherent noise frequencies still exist in the data; however, they are also of low amplitude. The total energy in these frequencies is very small; no adverse effects on data utility are expected.

Resolution estimation of TM-5 detectors produced results similar to TM-4 with IFOV values slightly larger than the specifications. This is expected to be due to a combination of smoothing because of processing effects plus atmospheric effects. Thermal calibration activities produced a method for obtaining a temperature for each digital count for TM-5.

REFERENCES

Anuta, P. E., Bartolucci, L. A., Dean, M. E., Lozano, D. F., Malaret, E., McGillem, C. D., Valdes, J. A., and Valenzuela, C. R., 1984. Landsat-4 MSS and Thematic Mapper Data Quality and Information Content Analysis: *IEEE Transactions on Geoscience and Remote Sensing*, v. GE-22 no. 3 pp. 222-236.

Bartolucci, L. A., Hoffer, R. M., and West, T. R., 1973. Computer-Aided Processing of Remotely Sensed Data for Temperature Mapping of Surface Water from Aircraft Altitudes: LARS Technical Report 042373, Purdue University, West Lafayette, IN.

Bartolucci, L. A., Anuta, P. E., and Lozano, D. F., 1985. Evaluation of TM-5 Thermal IR Band Radiometric Calibration for Water Temperature Mapping: *Proceedings 11th International Symposium on Machine Processing of Remotely Sensed Data*, LARS/Purdue Univ., West Lafayette, IN, June 25-27, (In press).

Bernstein, R., Lotspiech, J. B., Myers, H. J., Kolsky, H. G., and Lees, R. D., 1984. Analysis and Processing of Landsat-4 Sensor Data Using Advanced Image Processing Techniques and Technologies: *IEEE Transactions on Geoscience and Remote Sensing*, v. GE-22, no. 3, pp. 192-221.

Hughes Aircraft Co., 1985. Personal Communication Excerpted from a Paper by Jack C. Lansing and John Barker, 18 February, Goleta, CA.

Malaret, E., 1984. Methods for the Determination of the PSF and Restoration of Images in the Landsat-D Thematic Mapper: Ph.D. Dissertation Purdue University, School of Electrical Engineering, West Lafayette, IN.

Markham, B. L., and Barker, J. L., 1985. Spectral Characterization of the Landsat Thematic Mapper Sensors: NASA Conference Publication 2355, Vol. II—Thematic Mapper (TM), Part 1, pp. II-235-II-276.

McGillem, C. D., and Cooper, G. R., 1974. *Continuous and Discrete Signal and System Analysis:* Holt, Rinehart & Winston, New York, NY.

McGillem, C. D., Anuta, P. E., Malaret, E., and Yu, K. B., 1983. Estimation of a Remote Sensing System Point-Spread Function from Measured Imagery: *Proceedings 9th International Symposium on Machine Processing of Remotely Sensed Data*, LARS/Purdue University, West Lafayette, IN, 21-23 June, pp. 62-68.

McGillem, C. D., Malaret, E., and Anuta, P. E., 1984. Resolution Estimation for the Landsat-4 Thematic Mapper: *Proceedings Conference on Techniques for Extraction of Information from Remotely Sensed Images*, Society of Photographic Scientists and Engineers, Springfield, MD.

National Aeronautics and Space Administration, 1981. Application Notice for Participation in the Landsat-D Image Data Quality Analysis Program: 23 October.

National Aeronautics and Space Administration, 1983. Interface Control Document between NASA Goddard Space Center (GSFC) and Dept. of Interior, EROS Data Center (EDC) for Landsat-D, Computer Compatible Tape (CCT-AT, CCT-PT): NASA/Goddard Space Flight Center, Greenbelt, MD 20771, Rev. A, LSD-ICD-105, December.

Rosenfeld, A., and Kak, A., 1982. *Digital Picture Processing*, 2nd ed., Vol. 2, Academic Press, New York, NY.